Measurements of absolute *K*-shell ionization cross sections and *L*-shell x-ray production cross sections of Ge by electron impact

C. Merlet
ISTEEM, FU 160, CNRS, Université de Montpellier II, Sciences et Techniques du Languedoc, Place Eugene Bataillon, 34095 Montpellier Cedex 5, France

X. Llovet*
Serveis Cientificotècnics, Universitat de Barcelona. Lluís Solé i Sabarís 1-3, 08028 Barcelona, Spain

F. Salvat
Facultat de Física (ECM), Universitat de Barcelona, Diagonal 647, 08028 Barcelona, Spain
(Received 8 January 2004; published 18 March 2004)

Results from measurements of absolute *K*-shell ionization cross sections and $L\alpha$ x-ray production cross sections of Ge by impact of electrons with kinetic energies ranging from the ionization threshold up to 40 keV are presented. The cross sections were obtained by measuring $K\alpha$ and $L\alpha$ x-ray intensities emitted from ultrathin Ge films deposited onto self-supporting carbon backing films. Recorded x-ray intensities were converted to absolute cross sections by using estimated values of the sample thicknesses, the number of incident electrons, and the detector efficiency. Experimental data are compared with the results of widely used simple analytical formulas, with calculated cross sections obtained from the plane-wave and distorted-wave Born approximations and with experimental data from the literature.

DOI: 10.1103/PhysRevA.69.032708 PACS number(s): 34.80.Dp

I. INTRODUCTION

Accurate cross sections for ionization of inner atomic electron shells by electron impact are needed for multiple applications, such as materials characterization by electron probe microanalysis (EPMA) and Auger electron spectroscopy (AES), for the quantitative description of medical and industrial x-ray sources, and, in general, for the simulation of radiation transport in matter. Nevertheless, ionization cross-section data bases or predictive formulas required for these applications are not firmly established, especially for projectile electrons with kinetic energies near the ionization threshold.

Calculations of ionization cross sections within the plane-wave Born approximation (PWBA) provide reliable results for high-energy electrons. Near the ionization threshold, however, the PWBA is not adequate because it neglects the distortion caused by the atomic field on the wave function of the projectile and it also disregards electron exchange. Various semiempirical modifications to the PWBA have been proposed to account for these effects [1,2]. A more rigorous approach is to use the distorted-wave Born approximation (DWBA), in which the initial and final projectile wave functions include the distortion caused by the atomic field and, which also allows the description of exchange effects in a consistent way [3]. DWBA calculations are however extremely time consuming and, moreover, they are feasible only for a limited range of incident electron energies, which makes their use difficult in practical applications. Alternatively, empirical and semiempirical cross-section formulas have also been proposed [4].

The experimental measurement of inner-shell ionization cross sections has been a subject of continuing research for several decades. In spite of these studies, the body of available data is still scarce and the data are generally affected by important uncertainties. For example, absolute *L*-shell ionization cross sections have only been reported for Ar [5,6], Kr [7], and Xe [7,8], Au [9–13], W [13,14], and Pt [13]. The situation is even worse for *M* shells, for which experimental data are extremely rare. Moreover, for the elements and electron shells for which experimental data are available, one usually finds substantial disagreement between data from different sources, which are frequently larger than the uncertainties claimed by the authors [4,15]. It is, therefore, difficult to assess the reliability of calculated cross sections over a consistent set of elements, atomic shells, and incident electron energies, and the need for new, improved experimental measurements remains open.

In this paper we report experimental measurements of the *K*-shell ionization cross section and $L\alpha$ x-ray production cross section of Ge ($Z=32$) by impact of electrons with kinetic energies from the ionization threshold up to 40 keV. Cross sections were obtained by measuring $K\alpha$ and $L\alpha$ x-ray intensities emitted from ultrathin Ge films, which were deposited on self-supporting thin carbon backing films. X-ray measurements were performed using a wavelength-dispersive spectrometer (WDS) and a Si(Li) detector on two electron microprobe instruments. X-ray intensities were converted into absolute x-ray production cross sections by using estimated values of the sample thickness, the number of incident electrons, and the detector efficiency. In the case of *K*-shell ionization, x-ray production cross sections were fi-

*Author to whom correspondence should be addressed. Email address: xavier@giga.sct.ub.es

nally converted to ionization cross sections by using available values of the fluorescence yield and the x-ray emission rate. Our experimental results have been compared with two analytical formulas widely used in many applications, with theoretical cross sections calculated from the PWBA and DWBA and, wherever possible, with measurements from other authors. For comparison purposes, theoretical *L*-subshell ionization cross sections were converted to *L*-shell x-ray production cross sections by using relaxation data available from the literature.

II. METHOD

The methodology adopted for the present measurements is similar to that used in Ref. [16]. To obtain the x-ray production cross section σ_X we measured the flux $N_X(E)$ of characteristic x rays emitted from an ultrathin film of thickness t of the studied element, bombarded with N_e electrons of energy E. The x-ray production cross section is then obtained as

$$\sigma_X(E) = \frac{4\pi}{\mathcal{N}\, t\, N_e\, \epsilon\, \Delta\Omega} N_X(E), \tag{1}$$

where $\mathcal{N}$ is the density of atoms in the target (atoms per unit volume), $\Delta\Omega$ is the solid angle of collection, and ϵ is the spectrometer efficiency. Equation (1) assumes that electrons penetrate the film following a straight trajectory without losing energy. This assumption is plausible only for very thin films and for electron beams with relatively large energies.

The *K*-shell ionization cross section σ_K is obtained from the $K\alpha$ x-ray production cross section $\sigma_{K\alpha}$ as

$$\sigma_{K\alpha} = \frac{\Gamma_{L2,3-K}}{\Gamma_{Total-K}} \omega_K\, \sigma_K, \tag{2}$$

where $\Gamma_{L_{2,3}\text{-}K}$ and $\Gamma_{Total\text{-}K}$ are the x-ray emission rates for $K\alpha$ ($L_{2,3}$-K) transitions and for all possible (L,M,N-K) transitions, respectively, and ω_K is the fluorescence yield.

Vacancies in the L_i subshells can be produced not only by direct ionization, but also by radiative and non-radiative transitions to the *K* shell, Coster-Kronig transitions between L_i subshells and, to a lesser extent, by radiative transitions between L_i subshells. As a consequence, *L*-shell x-ray production cross sections are related to the ionization cross sections for all the L_i subshells and the *K* shell. The $L\alpha$ x-ray production cross section $\sigma_{L\alpha}$ is given by

$$\sigma_{L\alpha} = \frac{\Gamma_{M_{4,5}\text{-}L_3}}{\Gamma_{Total\text{-}L_3}} \omega_{L_3} [n_{KL_3}\sigma_K + \sigma_{L_3} + f_{23}\, \sigma_{L_2} + (f_{13} + f_{12}f_{23} + f'_{13})\sigma_{L_1}], \tag{3}$$

where $\Gamma_{M_{4,5}\text{-}L_3}$ and $\Gamma_{Total\text{-}L_3}$ are the x-ray emission rates for $L\alpha$ ($M_{4,5}$-L_3) transitions and for all possible (M,N,O-L_3) transitions, respectively. ω_{L_3} is the fluorescence yield for the L_3 shell, n_{KL_3} is the radiative plus nonradiative yield for transitions of vacancies from the *K* shell to the L_3 subshell, f_{12}, f_{13}, and f_{23} are the Coster-Kronig yields between *L* subshells, and f'_{13} is the intrashell radiative yield for transitions of vacancies from the L_1 subshell to the L_3 subshell. The contribution of intrashell radiative transitions of vacancies from the L_1 subshell to the L_2 subshell has not been included in Eq. (3) because of the extremely low value of the corresponding yield, f'_{12}. In the present work, we shall limit ourselves to measuring the $L\alpha$ x-ray production cross section: Eq. (3) will only be used to convert theoretical cross sections for impact ionization of the *K* shell and *L* subshells into $L\alpha$ x-ray production cross sections for comparison purposes.

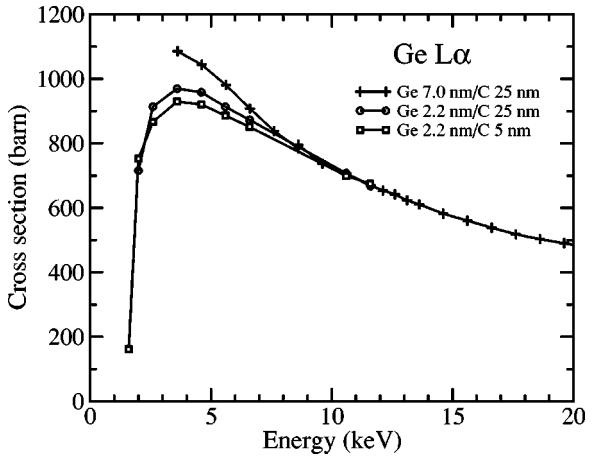

FIG. 1. Measured x-ray intensity vs electron incident energy for selected Ge/C samples with different thicknesses of the active and backing films.

III. EXPERIMENTAL TECHNIQUE

A. Sample preparation

The studied samples were Ge films deposited on carbon self-supporting backing films. Carbon was selected to hold the active Ge films because of its small backscattering effect and large tensile strength. The samples were produced as follows. First, carbon films of about 25 mm were evaporated on mica films. The mica films were separated from the carbon in distilled water. Carbon films floating on the water surface were then extracted with a grid of the kind used in transmission electron microscopy. Ge films were subsequently deposited onto the self-supporting carbon backing films. During the same evaporation runs, Ge twin films were also deposited onto thick polished ultrapure Fe targets. The Ge/Fe targets were used to determine the thickness of the Ge films by EPMA (see below). Electron micrographs and EPMA measurements of these targets did not show any indication of islanding of the evaporated metal.

In order to minimize the contribution of backscattered electrons from the backing carbon film, the thickness of the latter was reduced down to ~5 nm by ion milling, using the ion microprobe CAMECA IMS5F at the University of Montpellier. Ion milling of the sample was performed over a square raster of 80 μm. The effect of the backing-film thickness on the emitted x-ray intensity is illustrated in Fig. 1, which shows a comparison of the Ge $L\alpha$ x-ray intensity emitted from samples with different thickness of the Ge and

carbon backing films, as a function of the incident electron energy. We see that the thickness effect is appreciable for electron-beam energies below approximately 10 keV; the larger the Ge and/or backing film thickness, the higher the emitted intensity. This x-ray enhancement is due to electrons backscattered from the backing and/or scattered within the film, and it is more important for Ge $L\alpha$ than for Ge $K\alpha$ (for which it is almost negligible) due to the smaller ionization energies of the Ge *L* shells. To minimize the influence of the finite sample thickness on the shape of the measured cross-section curve, measurements of the $L\alpha$ x-ray emission cross section below 10 keV were performed on the thinnest film (with the thinnest carbon backing) available.

B. Apparatus

Cross sections were measured using two electron microprobes, namely a CAMECA SX-100 and a CAMECA SX-50 at the Universities of Montpellier and Barcelona, respectively. The first instrument is equipped with five wavelength-dispersive (WD) spectrometers while the second has four WD spectrometers and a Si(Li) detector. All WD spectrometers consist of several crystal monochromators and an argon-methane mixture proportional counter. According to the manufacturer's specifications, the Si(Li) diode is 3 mm thick, has an active area of 12.5 mm^2 and a 7-μm-thick beryllium window placed at the front of the detector. In both microprobes, a high-voltage generator provides the accelerating voltage and the beam, generated by an electron gun, is focused onto the target by means of a system of electromagnetic lenses. Conventional high-vacuum technology is used to prevent breakdown of the accelerating voltage and scattering of electrons in the beam by residual atoms. All the x-ray detection systems are oriented so as to collect x rays that emerge in directions forming an angle of 40° with the sample surface.

C. X-ray measurements with a WD spectrometer and a Si(Li)

Our strategy for absolute measurement of x-ray emission cross sections combines measurements with both spectrometers: the WD spectrometer is used to obtain relative values of the x-ray intensity as a function of the incident electron energy, while the Si(Li) detector is employed to obtain absolute x-ray intensities for a given value of the incident electron energy (typically 20 keV). In a final stage, the relative intensities are converted into absolute cross-sections by matching the cross-section value determined from the measurements with the Si(Li) detector. The reason for using the two detection systems is that the WD spectrometer has better energy resolution than the Si(Li) detector and therefore it yields higher peak-to-background ratios and thus, is more appropriate for measurements of x-ray intensities near the ionization threshold. However, the absolute efficiency of a WD spectrometer depends on the incoming photon wavelength in a rather complicated way [17], because both the solid angle and the crystal reflectivity largely depend on the photon energy. Conversely, the solid angle of detection of a Si(Li) detector is constant and its relative efficiency can be estimated more easily (see below).

With the WD spectrometer, x-ray intensities were measured from 1.62 keV to 40.62 keV in, at least, 1 keV steps. The value of the accelerating voltage was checked by measuring the cut-off of the bremsstrahlung spectrum. The monochromator crystals used were a LLiF (Large Lithium Fluorine) crystal for the measurement of Ge and Fe $K\alpha$ x rays, a TAP (Thallium Acid Phtalate) crystal for Fe and Ge $L\alpha$ x-rays, and a Ni-C multilayer crystal (referred to as PC2) for the measurement of C $K\alpha$ x-rays (see below). Electron currents were selected to reach a compromise between x-ray counting rate and film damage, with typical values of 100 nA. Measurements were performed on the wavelength channel corresponding to the maximum of the characteristic peak and the background was subtracted by linear interpolation of x-ray measurements on channels at both sides of the peak. For each accelerating voltage, measurements were performed at, at least, two positions on five different self-supporting films, with counting times typically of 100 s at each position. Thus the standard deviation for the set of measurements not only accounted for uncertainties due to counting statistics, but also for errors arising from possible inhomogeneities in the active film thickness.

The interaction of electrons and x rays with the supporting grid and the specimen stage, and to a lesser extent with the specimen chamber, originates stray radiation that may enhance the recorded x-ray intensity. The effect of stray radiation is important especially for the measurement of Ge $L\alpha$ x rays due to the small ionization energies of the *L* subshells. To reduce stray radiation, a Faraday cup was placed below the sample and aligned with the electron beam to absorb transmitted electrons and x rays. The cup consisted of an 8-mm-diameter carbon cylinder with 0.5-mm-thick and 2 -cm-long Be lids, in which the upper lid had a 2.5-mm -diameter hole. Measurements on self-supporting carbon foils (with no active layer) showed no spurious peaks near the Ge $L\alpha$ and $K\alpha$ peaks. During the cross-section measurements, C $K\alpha$ x rays from the carbon backing film were also recorded. It was assumed that a variation of the C $K\alpha$ intensity with respect to that obtained from a standard backing film was due to either stray radiation, target damage, or wrinkling by the electron beam or instrumental drift, and the corresponding Ge measurements were rejected. Finally, to avoid contamination during the long measurement times, a liquid-nitrogen cold finger was used.

For measurements with the Si(Li) detector, beam currents were chosen to yield dead-time counting losses less than 1–2 %. Probe currents were measured with a Faraday cup placed on the sample holder, and the number of incident electrons N_e was evaluated by multiplying the probe current I_0 by the "live" acquisition time, determined by the Si(Li) detector software. Measurement times were typically about 4000 per spectrum, which ensures that the statistical uncertainty of the x-ray peaks is less than 2 %. Peak intensities were obtained by measuring the area of the corresponding peak after subtracting the background, which was determined using a polynomial fit. To minimize stray radiation coming from elsewhere in the specimen chamber, the emerging photon beam was collimated with a 0.3-mm-diameter diaphragm placed in front of the beryllium window, at 53 mm from the specimen.

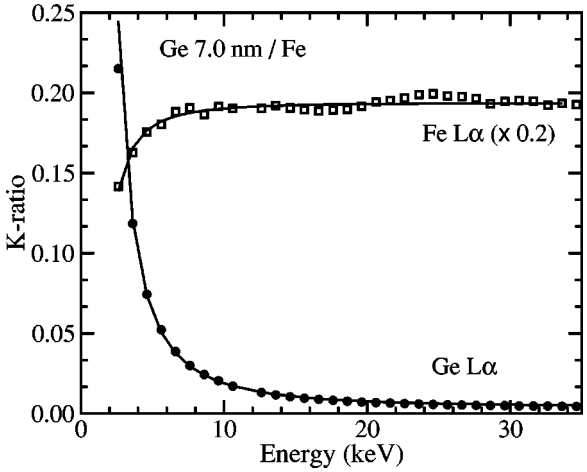

FIG. 2. *K*-ratios for Ge $L\alpha$ and Fe $K\alpha$ x-ray lines from a 7.0-nm-thick Ge film on a Fe substrate, as functions of the kinetic energy of the incident electron beam. The *K*-ratios were determined with respect to pure Ge and Fe, respectively. Symbols represent experimental data. Curves are results from the x-ray emission model of Merlet [18], which was used for thickness determination.

D. Thickness determination

To determine the thickness of the Ge films used in the experiments, EPMA measurements were performed at varying electron energies on the samples with twin Ge films deposited on Fe substrates. We measured the Ge and Fe $L\alpha$ and the Fe $K\alpha$ x-ray intensities from the above-mentioned samples, as well as from standards of these elements, from 2.6 keV up to 34.62 keV. In EPMA terminology, the ratio of the x-ray intensity from an unknown sample to that from a standard target (with known composition) is usually referred to as the *k* ratio. Measured *k* ratios were then analyzed with the help of an EPMA code [18], which calculates the thickness and composition of a thin film deposited on a substrate by least-squares fitting of an analytical x-ray emission model to the measured intensities (see Fig. 2). It is worth mentioning that when the atomic numbers of the layer and the substrate are similar (which is the case for the specimens considered here), the accuracy of the thickness determination provided by this EPMA technique and code is better than 5 % [18]. The thicknesses of the Ge films were found to be in the range between 1 and 10 nm.

E. Si(Li) efficiency determination

The absolute efficiency of a Si(Li) detector can be considered to be the product of its intrinsic efficiency and the collection solid angle. For photons with energies in the interval from ~3 keV to ~15 keV, it is plausible to assume that the intrinsic efficiency is equal to unity (see, e.g; Ref. [19]). Therefore, in this region, the absolute efficiency will be directly determined by the collection solid angle. This assumption, however, is no longer valid below ~3 keV mainly because of the increasing importance of x-ray absorption in the detector Be window, the Au contact layer, and in the so-called Si dead layer. As a result, the intrinsic efficiency drops suddenly when the energy decreases.

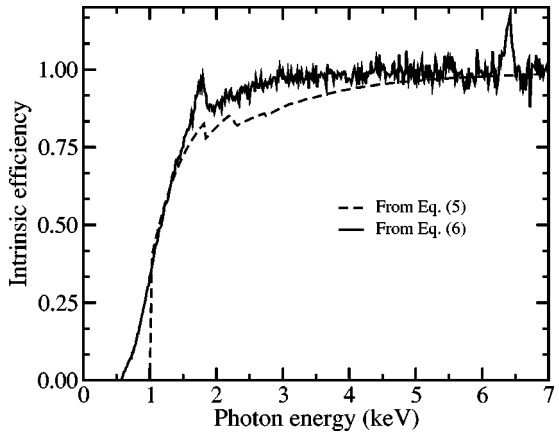

FIG. 3. Estimated intrinsic detector efficiency of the Si(Li) detector as a function of emitted photon energy using the approaches described in Eq. (5) and (6).

In this paper we have determined the detector efficiency at the photon energy of the Ge $L\alpha$ x-ray line (1.188 keV) as follows. Let us consider a thick target irradiated with an electron beam of energy E_0. The number $N_{\mathrm{exp}}(E)$ of photons detected per unit energy interval and unit solid angle per incident electron is

$$N_{\mathrm{exp}}(E) = \frac{N_{\mathrm{ch}}(E)}{N_{\mathrm{e}}\ \epsilon(E)\Delta\Omega\ \Delta E}, \tag{4}$$

where $N_{\mathrm{ch}}(E)$ is the number of experimental counts in a particular photon energy channel of width ΔE centered at E, and N_{e} is the number of incident electrons. If we replace $N_{\mathrm{exp}}(E)$ by the result from a Monte Carlo (MC) simulation expressed in absolute units (N_{MC}), then $\epsilon(E)$ can be calculated as

$$\epsilon(E) = \frac{N_{\mathrm{ch}}(E)}{N_{\mathrm{e}}\ N_{\mathrm{MC}}(E)\Delta E\ \Delta\Omega}. \tag{5}$$

In a previous study [20], we showed that simulated thick-target bremsstrahlung (TTB) spectra from pure carbon targets, obtained with the aid of the MC code PENELOPE [21], were in excellent agreement with absolute x-ray spectra measured with the Si(Li) detector in the energy range 3–15 keV, assuming that the intrinsic efficiency in this range is unity. Here we will take advantage of the fact that the scattering cross sections and simulation algorithm implemented in PENELOPE are expected to be valid below 3 keV, and we will use results from MC simulations with this code to estimate the drop of the detector efficiency. For this purpose, we have measured and simulated TTB spectra from different low-atomic-number targets, namely carbon, boron, and beryllium, and we have used Eq. (5) to obtain the detector efficiency at the photon energy of 1.188 keV. Figure 3 compares the resulting efficiency with that obtained from assuming pure exponential attenuation of the photon beam in the Be window, the Au contact layer, and the Si dead layer [22], i.e.,

TABLE I. Measured *K*-shell ionization cross sections and $L\alpha$ x-ray production cross sections of Ge by electron impact.

Energy (keV)	Ge *K*-shell Cross section (barn)	Ge $L\alpha$ Cross section (barn)
1.62		163
2.00		759
2.62		874
3.62		937
4.62		929
5.62		894
6.62		857
7.62		820
8.62		781
9.62		742
10.62		714
11.62	28	675
12.12	51	659
12.62	70	647
13.12	89	628
13.62	104	616
14.62	131	586
15.62	152	564
16.62	170	543
17.62	186	523
18.62	201	511
19.62	212	495
20.62	222	482
21.62	230	467
22.62	237	455
23.62	244	442
24.62	249	430
25.62	254	420
26.62	256	409
27.62	260	399
28.62	261	386
29.62	262	377
30.62	264	364
31.62	267	363
32.62	264	352
33.62	267	344
34.62	269	340
35.62	270	333
36.62	270	325
37.62	271	322
38.62	271	316
39.62	272	307
40.62	270	304

$$\epsilon(E) = \exp[-[\mu_{\mathrm{Be}}(E)t_{\mathrm{Be}} + \mu_{\mathrm{Au}}(E)t_{\mathrm{Au}} + \mu_{\mathrm{Si}}(E)t_{\mathrm{Si}}]], \quad (6)$$

where μ_{Be}, μ_{Au}, and μ_{Si} are mass absorption coefficients for Be, Au, and Si (which have been taken from the PENELOPE database) and t_{Be}, t_{Au}, t_{Si} are the thicknesses of the Be window, the Au contact layer, and the Si dead layer, respectively (for which we have adopted the values provided by the manufacturer). We see that at the energy of interest of 1.188 keV, the intrinsic efficiencies estimated by both methods agree closely.

F. Uncertainties in the measurements

Cross-section measurements are affected by random uncertainties arising mainly from counting statistics, background substraction, sample nonuniformity, stray radiation, and instrumental drift during measurements. From repeated measurements, random uncertainties were estimated to be less than 2 %. It is worth pointing out that random uncertainties affect the shape of the cross-section curves. The conversion from relative cross sections to absolute cross sections introduces additional uncertainties of a systematic nature, which are the same for all incident electron energies. These are mainly uncertainties in the estimation of target thicknesses (5 %), detection efficiency (5 %), number of incident electrons (2 %), and the statistical uncertainties of the measurements with the Si(Li) detector at 20 keV (2 %). In the determination of the Ge *K*-shell cross section, added to these are the uncertainties of the adopted fluorescence yields (3 %) and x-ray emission rates (2 %) (see below). The global uncertainties, obtained by adding the random and systematic uncertainties in quadrature, were about 9 % for the *K*-shell ionization cross section and 8 % for the Lα x-ray production cross section.

IV. RESULTS AND DISCUSSION

In this section, we present the results from our measurements, which are summarized in Table I, and compare them with the predictions of two theoretical calculations, with two analytical formulas and with experimental measurements by other authors, when available. The first theoretical calculation is the PWBA described by Mayol and Salvat [1]. In their approach, the generalized oscillator strength is obtained from the cross section for photoelectric absorption of photons in the considered atomic shell; the formulation also incorporates exchange corrections, through the Ochkur approximation, and an empirical Coulomb correction. The second theoretical approach considered here is the DWBA, as implemented in a robust calculation algorithm developed recently by Segui *et al.* [3]. As mentioned previously, in the DWBA, the wave functions for the initial and final states of the projectile include the distortion caused by the atomic field; this feature allows the description of exchange effects in a consistent way. The analytical formulas selected for comparison purposes are those of Casnati *et al.* [23] and Gryzinski [24], which are widely used in many applications.

A. *K*-shell ionization

For the determination of the Ge *K*-shell ionization cross section, the fluorescence yield ω_{K} was taken from the compilation by Hubbell *et al.* [25]; its uncertainty is estimated to be about 2 % The value of the x-ray emission rate was taken from Scofield [26]. Explicitly, the values adopted in the present work are $\omega_{\mathrm{K}}=0.523$ and $\Gamma_{\mathrm{L_{2,3}\text{-}K}}/\Gamma_{\mathrm{Total\text{-}K}}=0.8680$.

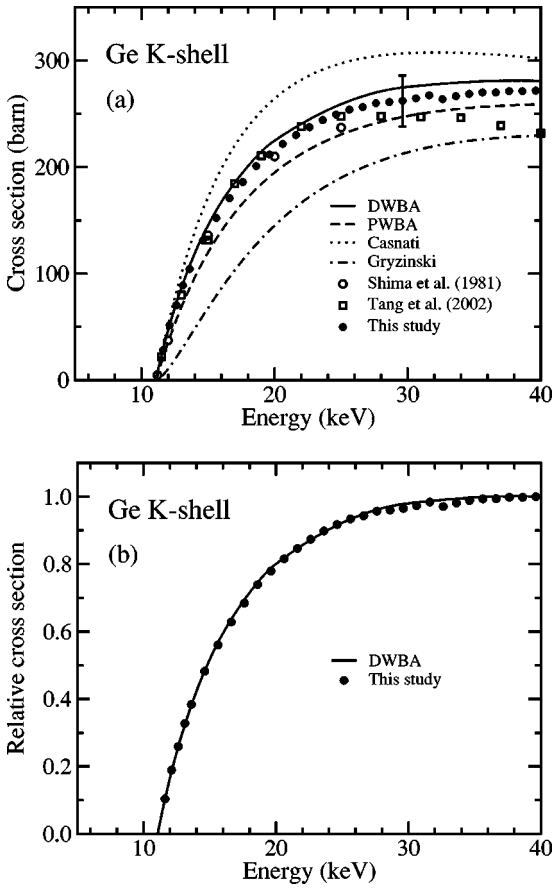

FIG. 4. Absolute (a) and relative (b) *K*-shell ionization cross section vs incident electron energy for Ge. The dashed curves indicate the PWBA calculation results from Mayol and Salvat's model; dotted curves, the formula of Casnati *et al.* [23]; dot-dashed curves, the formula of Gryzinski [24]; solid curves represent the DWBA calculation of Segui *et al.* [3]. Full circles are results from the present measurements. Other symbols represent measurements by the authors indicated in the legends. The relative cross sections in (b) have been normalized to unit maximum value.

Figure 4(a) compares our experimental measurements with the PWBA and DWBA calculations of Mayol and Salvat [1] and Segui *et al.* [3], respectively, the analytical formulas of Gryzinski [24] and Casnati *et al.* [23], and the experimental measurements of Shima *et al.* [11] and Tang *et al.* [27]. Our measured values lie between the DWBA and PWBA calculations, and agree with both calculations within experimental uncertainties. The agreement with the DWBA calculation seems to improve when the electron energy approaches the ionization threshold. The formulas of Casnati and Gryzinki give results that are systematically higher and lower, respectively, than our measurements. Our data also agree reasonably with those of Shima *et al.* [11]; the measurements of Tang *et al.* [27] decrease more rapidly than ours with increasing incident electron energies.

As mentioned above, the global uncertainties of the present experimental data are of the order of 9 %. Note, however, that the shape of the cross-section curve (i.e., the relative cross-section values) is much more accurate, because it is only affected by relative uncertainties (which are less than 2 %). This is illustrated in Fig. 4(b) where the experimental and DWBA-based calculated cross sections have been normalized to the corresponding maxima. The good agreement between both cross-section data is noteworthy.

TABLE II. The x-ray emission rate, fluorescence yield, radiative, and nonradiative yields for transitions of vacancies from the *K* shell to the L_3 subshell, Coster-Kronig yields between *L* subshells and the intrashell radiative yield for transitions of vacancies from the L_1 subshell to the L_3 subshell used in this work, taken from Scofield [26], Krause [28], and Rao *et al.* [30].

$\Gamma_{M_{4,5}\text{-}L_3}/\Gamma_{\text{Total-}L_3}$	ω_{L_3}	n_{KL_3}	f_{12}	f_{13}	f_{23}	f'_{13}
0.953	0.015	0.644	0.28	0.53	0.050	3.2×10^{-5}

B. *L*-shell x-ray production

L-shell ionization cross sections obtained from the above mentioned calculations and analytical formulas have been

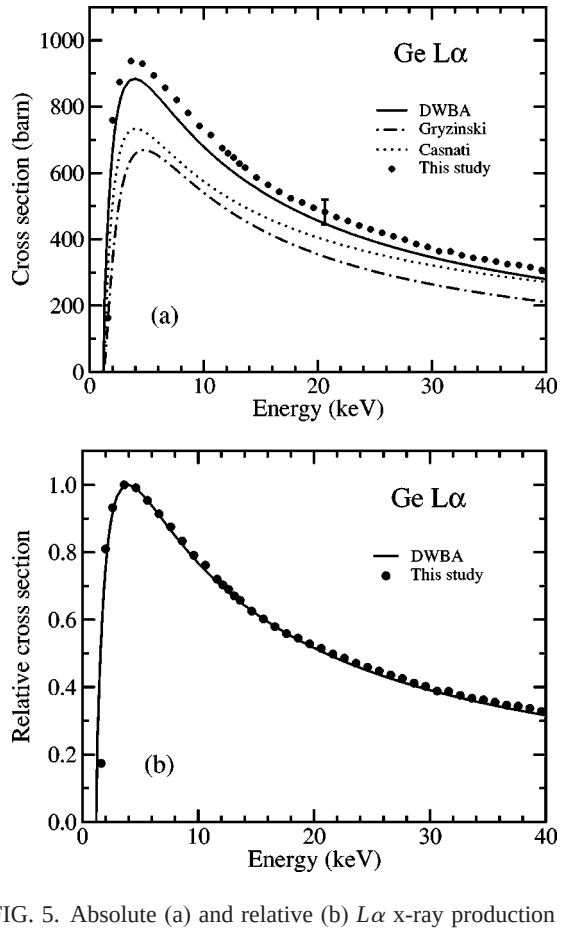

FIG. 5. Absolute (a) and relative (b) $L\alpha$ x-ray production cross sections vs incident electron energy for Ge. The curves have been obtained by means of Eq. (3) using ionization cross sections calculated from different formulas and approximations. The dotted curves indicate results from the formula of Casnati *et al.* [23]; dot-dashed curves, the formula of Gryzinski [24]; continuous curves represent the DWBA calculation of Segui *et al.* [3]. Full circles are results from the present measurements. The relative cross sections in (b) have been normalized to unit maximum value.

converted into $L\alpha$ x-ray production cross sections by using Eq. (3). For Ge, x-ray fluorescence and Coster-Kronig yields are available from two different bibliographic sources [28,29]. For a given set of theoretical *L*-shell ionization cross sections, the $L\alpha$ x-ray production cross sections obtained with the yields from both sources were found to differ by about 5 %. These yields however, may be affected by larger uncertainties. Indeed, Krause conservatively recommends 20 % uncertainty for ω_{L3}, 15 % for f_{12}, 10 % for f_{13}, and 20–30 % for f_{23}. In order to facilitate the comparison, we have adopted the fractional emission rate given by Scofield [26], the fluorescence, Coster-Kronig and intrashell radiative yields given by Krause [28], and the radiative and nonradiative yield for vacancies of the *K* shell to the L_3 subshell given by Rao *et al.* [30], which are summarized in Table II.

Figure 5(a) compares our Ge $L\alpha$ cross section measurements with the DWBA calculations of Segui *et al.* [3] and the analytical formulas of Gryzinski and Casnati *et al.* No experimental measurements were found in the literature to compare our results with. We can see that for all incident electron energies our data lie systematically higher than the DWBA calculation, although almost within the limits of the experimental error bars. The formulas of Casnati and Gryzinki give results that are systematically much lower than our measurements. Again, when we normalize the experimental and DWBA calculated cross sections to their respective maxima, Fig. 5(b), the agreement is seen to be excellent.

V. CONCLUSION

In conclusion, we have performed measurements of electron-impact *K*-shell ionization and *L*-shell x-ray production cross sections of Ge by electron impact, for projectiles with kinetic energies from the ionization threshold up to 40 keV. With the improvements in the experimental procedure, we have been able to reduce the relative and absolute uncertainties of the cross-section measurements down to 2 % and 8–9 %, respectively. We have also shown that the predictions of the DWBA algorithm developed by Segui *et al.* [3] are in good agreement with our experimental data.

ACKNOWLEDGMENTS

We would like to thank Dr. Cristiani S. Campos for her help with the DWBA calculations. This work was partially supported by the Spanish Fondo de Investigación Sanitaria (Project No. PI030676). Financial support from the PICASSO programme (Project No. HF2000-0053) is gratefully acknowledged.

[1] R. Mayol and F. Salvat, J. Phys. B **23**, 2117 (1990).
[2] R. Hippler, Phys. Lett. A **144**, 81 (1990).
[3] S. Segui, M. Dingfelder, and F. Salvat, Phys. Rev. A **67**, 062710 (2003).
[4] C. J. Powell, in *Electron Impact Ionization*, edited by T. D. Mark and D. H. Dunn (Springer-Verlag, Berlin, 1985), Chap. 6.
[5] A. Langenberg, F. J. de Heer, and J. van Eck, J. Phys. B **8**, 2079 (1975).
[6] R. Hippler, H. Klar, K. Saeed, I. McGregor, A. J. Duncan, and H. Kleinpoppen, J. Phys. B **16**, L617 (1983).
[7] C. A. Quarles and M. Semaan, Phys. Rev. A **26**, 3147 (1982).
[8] R. Hippler, I. McGregor, M. Aydinol, and H. Kleinpoppen, Phys. Rev. A **23**, 1730 (1981).
[9] S. I. Salem and L. D. Moreland, Phys. Lett. **37A**, 161 (1971).
[10] D. V. Davis, V. D. Mistry, and C. A. Quarles, Phys. Lett. **38A**, 169 (1972).
[11] K. Shima, T. Nakagawa, K. Umetani, and T. Mikumo, Phys. Rev. A **24**, 72 (1981).
[12] H. Schneider, I. Tobehn, F. Ebel, and R. Hippler, Phys. Rev. Lett. **71**, 2707 (1993).
[13] C. S. Campos, M. A.Z. Vasconcellos, X. Llovet, and F. Salvat, Phys. Rev. A **66** 012719 (2002).
[14] C. N. Chang, Phys. Rev. A **19**, 1930 (1979).
[15] C. J. Powell, in *Microbeam Analysis*, edited by J. R. Michael and P. Ingram (San Francisco Press, San Francisco, 1990).
[16] X. Llovet, C. Merlet, and F. Salvat, J. Phys. B **33**, 3761 (2000).
[17] S. Reusch, H. Genz, W. Löw, and A. Richter, Z. Phys. D: At., Mol. Clusters **3**, 379 (1986).
[18] C. Merlet, in *Proceedings of the 29th Annual Conference of the Microbeam Analysis Society*, edited by E. S. Etz (VCH Publishers, New York, 1995), p. 203.
[19] J. H. Paterson, J. N. Chapman, W. A.P. Nicholson, and J. M. Titchmarsh, J. Microsc. **154**, 1 (1988).
[20] E. Acosta, X. Llovet, and F. Salvat, Appl. Phys. Lett. **80**, 2328 (2002).
[21] F. Salvat, J. M. Fernández-Varea, and J. Sempau, Computer Code PENELOPE (OECD/NEA Data Bank, Issy-les-Moulineaux, France, 2003).
[22] P. J. Statham, J. Microsc. **123**, 1 (1981).
[23] E. Casnati, A. Tartari, and C. Baraldi, J. Phys. B **15**, 155 (1982).
[24] M. Gryzinski, Phys. Rev. **138**, 336 (1965).
[25] J. H. Hubbell, P. N. Trehan, N. Singh, B. Chand, D. Mehta, M. L. Garg, R. R. Garg, S. Singh, and S. Puri, J. Phys. Chem. Ref. Data **23**, 339 (1994).
[26] J. H. Scofield, Phys. Rev. **179**, 9 (1969).
[27] C. Tang, Z. An, Z. Luo, and M. Liu, J. Appl. Phys. **91**, 6739 (2002).
[28] M. O. Krause, J. Phys. Chem. Ref. Data **8**, 307 (1979).
[29] S. Puri, D. Mehta, B. Chand, N. Singh, and P. Trehan, X-Ray Spectrom. **22**, 358 (1993).
[30] P. V. Rao, M. H. Chen, and B. Crasemann, Phys. Rev. A **5**, 997 (1972).